Experimental and theoretical study of free induction decay of water molecules induced by terahertz laser pulses

Philippe Babilotte,[1] Laurent H. Coudert,[2] Franck Billard,[1] Edouard Hertz,[1] Olivier Faucher,[1] and Bruno Lavorel[1]

[1]*Laboratoire Interdisciplinaire Carnot de Bourgogne, UMR 6303 CNRS-Université Bourgogne Franche-Comté, BP 47870, 21078 Dijon Cedex, France*

[2]*Institut des Sciences Moléculaires d'Orsay (ISMO), CNRS, Univ. Paris-Sud, Université Paris-Saclay, F-91405 Orsay, France*

(Received 11 January 2017; published 10 April 2017)

We experimentally investigate the free induction decay in the asymmetric top molecule H_2O after interaction with short terahertz pulses. Two different experimental techniques are used to perform measurements in the gas phase under different experimental conditions: electro-optical detection and terahertz field-induced second-harmonic generation. Simulations of the free induction decay signals are performed with a theoretical approach in which the absorption and dispersion coefficients are evaluated from spectroscopic data pertaining to the water molecule. Experimental and theoretical signals are compared directly in the time domain in two limiting cases. For a short propagation length of ∼40 cm, both signals show a slightly altered electric field consistent with the approximation of weak absorption and dispersion. For a longer propagation length of ∼300 cm, the electric field is heavily distorted. A good agreement between experimental and calculated signals is obtained in both cases. Finally, we discuss the advantages and/or disadvantages of the two experimental techniques.

DOI: 10.1103/PhysRevA.95.043408

I. INTRODUCTION

Free induction decay (FID) of gas-phase water molecules excited by THz pulses has been reported in a number of works. Pioneering studies have been performed at room temperature [1] and in flames [2]. More recently, the H_2O FID has been studied as a function of humidity [3] and for atmospheric transmission [4–7]. In laboratory measurements, absorption of H_2O is so strong that, even at room temperature, propagation in air gives rise to strong attenuation of THz pulses and large FID signals. In cases where THz pulses are applied to other gases, the signal originating from water molecules interferes with the original signal. Accurate simulation of the FID signal is required in order to predict the interaction of the composite THz electric field (initial pulse followed by water FID) with another molecule. For example, this effect has been investigated in an OCS molecule [8]. In the present work, the FID signal of water molecules is measured at room temperature for several propagation lengths with two different techniques. Our goal is to compare directly in the time domain the observed signals with accurate simulations. Note that THz studies of asymmetric top molecules such as water are generally considered in the frequency domain by performing the Fourier transform of the temporal FID signal. The absorption and dispersion of the sample are then deduced in the terahertz range. Only two recent works show a comparison between experimental data and simulations in the time domain [6,9]. In Ref. [6], the measured THz pulse transmitted through atmosphere for a 6.18-m-long path is compared with the calculated pulse, taking into account refractivity and absorption of water molecules. In Ref. [9], time-dependent orientation and alignment of the SO_2 molecule are studied. Based on parameters available in a spectroscopic data base, the propagation of the terahertz pulse is simulated and the results are successfully compared with the FID temporal signals recorded using both techniques. A satisfactory agreement is obtained even for time delays up to 80 ps and advantages and/or disadvantages of the two techniques are discussed.

The paper is organized as follows. In Sec. II, the experimental setup is described, including the THz source and the two detection schemes. The numerical simulation of the H_2O FID signal is detailed in Sec. III. We show in Sec. IV comparisons between simulated and experimental temporal FID signals of the water molecule. Finally, conclusions are given in Sec. V.

II. EXPERIMENTAL SETUP

The experimental setup depicted in Fig. 1 consists of a unit to produce THz pulses combined with two different detection devices. The THz pulses are produced through plasma generation in air with two-color femtosecond pulses [10–15]. To that end, a part of a chirp-pulse amplifier (CPA), delivering 100-fs pulses at 800 nm with 7.5-mJ energy, is focused in atmospheric air. A type-I phase-matching β-barium borate (BBO) crystal, inserted between the focusing lens and the focal point, creates the second harmonic at 400 nm. The energy of the THz pulses produced by the combination of the fundamental beam and its second harmonic is optimized, adjusting the phase-matching angle of the frequency-doubling crystal and its longitudinal position. The pulse duration of the emitted THz pulses is a few hundred femtoseconds and their shape is close to a single-cycle pulse. After collimation by an off-axis parabolic mirror, the two beams at 800 and 400 nm are filtered out by means of a homemade filter (2-mm-thick plate from polytetrafluoroethylene and a thin black polyethylene sheet). The THz pulses propagate in atmospheric air, leading to the excitation of the water molecules and subsequent reemission of a secondary THz radiation (FID). The terahertz electric field after collimation is less than 1 kV/cm. The partial pressure of H_2O is around 1.15×10^{-2} atm (50% humidity). The total THz radiation, including the initial THz pulse modified by the propagation and followed by the FID of H_2O, is collected and sent to the detection devices.

As mentioned above, the measurement of the THz field makes use of two devices. The first one is based on the

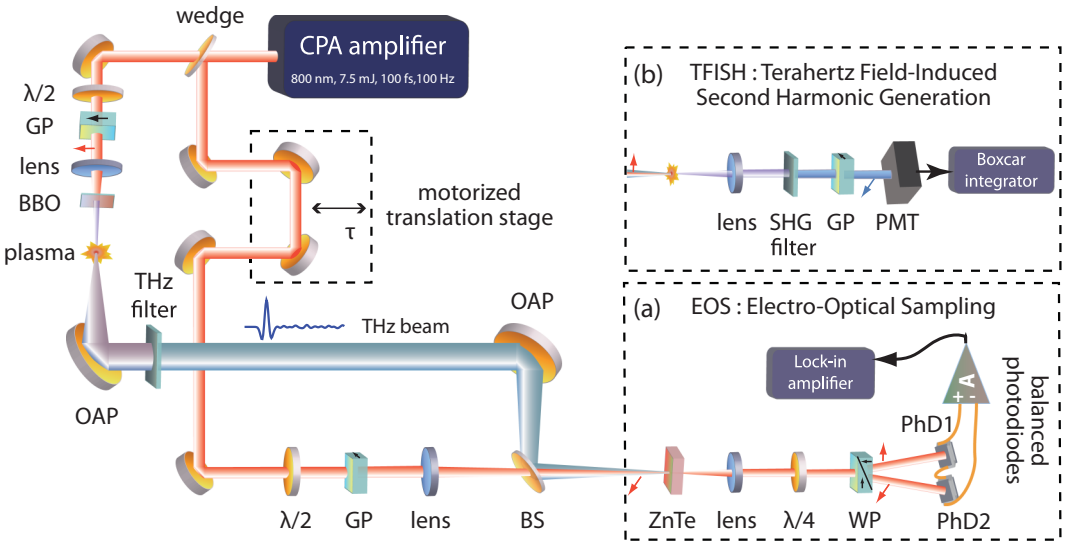

FIG. 1. Experimental setup. Chirp-pulse amplifier (CPA). $\lambda/2$: half-wave plate. $\lambda/4$: quarter-wave plate. GP: Glan prism polarizer. BBO: β-barium borate crystal. THz filter: see the text. OAP: off-axis parabolic mirror. BS: indium tin oxide beamsplitter. ZnTe: electro-optical crystal. WP: Wollaston prism. PhD1 and PhD2: balanced photodiodes. A: integrated amplifier. PMT: photomultiplier tube. The detection device is either based on (a) electro-optical sampling (EOS) or (b) terahertz field-induced second-harmonic generation (TFISH).

electro-optical temporal sampling (EOS) of the THz radiation [16–19]. A weak probe beam (typically ∼5 nJ) derived from the chirp-pulse amplifier is focused and spatially overlapped with the THz radiation in a ZnTe (110) crystal. In that case, the polarization of the probe beam is modified through the Pockels effect induced by the THz beam. The change of polarization is measured by combining a quarter-wave plate (QWP), a Wollaston prism (WP), and two head-to-tail connected photodiodes. The quarter-wave plate is oriented so as to obtain a circular polarization without a THz pulse providing equivalent signals for the two photodiodes. The differential signal in the presence of the THz pulse is directly proportional to its electric field $E(t)$ at a given time t and at the point where the ZnTe crystal is located. $E(t)$ is then sampled by changing the time delay between the two pulses with a motorized delay line stage. After amplification, the differential signal is connected to a lock-in amplifier synchronized with the laser repetition rate.

The EOS signal recorded by the lock-in amplifier is proportional to ΔI, the difference between the optical intensities measured by the two head-to-tail connected photodiodes. ΔI is given by [19]

$$S_{\mathrm{EOS}} \propto \Delta I = I_{\mathrm{probe}}\, \omega\, n^3\, E(t)\, r_{41} \frac{L}{c}, \qquad (1)$$

where I_{probe} is the probe intensity, ω the probe angular frequency, n the refractive index at the probe frequency, $r_{41} = 4$ pm/V the electro-optic coefficient of the ZnTe crystal, $L = 200$ μm the crystal length, and c the speed of light in vacuum. Note that $E(t)$ in Eq. (1) is the total electric field including the transmitted THz pulse $E_0(z,t)$ and the FID electric field, as discussed below. It should be emphasized that in the case of a long interaction path as considered here, and consequently of a relatively strong absorption, the FID signal is not exactly proportional to the time derivative of the degree of orientation, as observed in Refs. [9,15,20]. The proportionality between these two quantities comes from the assumption that the initial THz pulse is not affected through propagation in the molecular sample [15]. This assumption is not valid in the cases discussed in the present work.

The second device to measure the FID signals is based on second-harmonic generation in air plasma. It relies on a third-order nonlinear frequency mixing process, called terahertz field-induced second-harmonic generation (TFISH). The method, first reported in liquids [21], has demonstrated its effectiveness in detecting THz radiations with a large bandwidth in various gaseous media [22,23]. In this technique, the probe beam at 800 nm is much more intense than in the EOS scheme. Frequency mixing between the THz radiation and the fundamental probe radiation leads to the generation of 400-nm light. After filtering the fundamental frequency, the TFISH signal is detected by a photomultiplier (PM) and recorded with a boxcar integrator. The signal delivered by the PM is proportional to the THz field squared, $S_{\mathrm{TFISH}} \propto E(t)^2$. Simultaneously, other nonlinear optical processes can also contribute to the second-harmonic generation and can then be used as a local oscillator for heterodyne TFISH detection [24]. In the present case, the probe energy is intense enough to produce plasma in air, and the local oscillator is the second-harmonic generation related to free electrons. More precisely, the local oscillator originates from the following processes. The probe beam first ionizes molecules in air (mainly oxygen because of its low ionization potential). Due to the transverse spatial profile of the probe beam, a radial gradient of free electron density is produced. The second-order optical response of this electronic gradient gives rise to second-harmonic generation. This additional contribution does not depend on the THz field itself [25–28]. It provides us with a means to improve the sensitivity of the THz detection. The TFISH signal taking into account the local oscillator E_{LO} is given by

$$S_{\mathrm{TFISH}} \propto [E(t) + E_{\mathrm{LO}}]^2. \qquad (2)$$

III. NUMERICAL SIMULATION

The results reported by Harde and Grischkowsky [29] concerning the propagation of a THz pulse were obtained solving the Maxwell-Bloch equations in the low-intensity limit. These results will be used for simulating the electric field at various distances z from the region where the terahertz pulse is produced. Assuming that the electric field of the terahertz pulse is along the space-fixed x axis, Eq. (9) of Harde and Grischkowsky [29], reproduced below, allows us to express its amplitude $E(z,t)$ in terms of $E(\omega)$, the Fourier transform of the initial field at $z = 0$:

$$E(z,t) = \int_{-\infty}^{+\infty} E(\omega)\exp[-i(\omega t - k_0 z)] \times \exp[i\Delta k(\omega)z]\exp\left[-\frac{1}{2}\alpha(\omega)z\right]d\omega, \quad (3)$$

where $\alpha(\omega)$ is the absorption coefficient, $\Delta k(\omega)$ is the dispersion coefficient, and k_0 is the wave vector equal to ω/c. For a single line i, the absorption coefficient $\alpha_i(\omega)$ is

$$\alpha_i(\omega) = N S_i(T) f(\omega,\omega_i), \quad (4)$$

where N is the number density, T is the temperature, $S_i(T)$ is the temperature-dependent line intensity, and $f(\omega,\omega_i)$ is the line shape depending on the transition angular frequency ω_i. In agreement with Grischkowsky and co-workers [6,7,29,30] and Rosenkranz [31], the following line shape is taken:

$$f(\omega,\omega_i) = \frac{1}{\pi}\left(\frac{\omega}{\omega_i}\right)^2\left(\frac{\Delta\omega_i}{(\omega-\omega_i)^2+\Delta\omega_i^2} + \frac{\Delta\omega_i}{(\omega+\omega_i)^2+\Delta\omega_i^2}\right), \quad (5)$$

where $\Delta\omega_i$ is the line half-width at half maximum. Similarly, the dispersion for a single line $\Delta k_i(\omega)$ is equal to

$$\Delta k_i(\omega) = N S_i(T)\frac{\omega}{\pi\left(\omega_i^2-\omega^2\right)}g(\omega,\omega_i), \quad (6)$$

where $g(\omega,\omega_i)$ is

$$g(\omega,\omega_i) = 1 - \frac{\omega\Delta\omega_i^2}{2\omega_i^2} \times\left[\frac{\omega+\omega_i}{(\omega-\omega_i)^2+\Delta\omega_i^2} + \frac{\omega-\omega_i}{(\omega+\omega_i)^2+\Delta\omega_i^2}\right]. \quad (7)$$

Due to the form of Eqs. (4)–(7), the absorption (dispersion) coefficient is an even (odd) function of ω.

The absorption and dispersion coefficients can now be obtained, summing $\alpha_i(\omega)$ and $\Delta k_i(\omega)$ in Eqs. (4) and (6), respectively, over all lines i. For practical purposes, the summation is restricted to transitions with upper and lower values of the rotational quantum number J smaller than a maximum value J_{Max}. The electric field can then be computed using Eq. (3) for any z value. Although not done in the present investigation, the dispersion and absorption coefficients also allow us to retrieve the complex electric susceptibility $\chi(\omega)$, with the help of Eqs. (7) and (8) of Harde and Grischkowsky [29], and $P(z,t)$ the polarization using their Eq. (5). Information about the molecular orientation can then be extracted, since the polarization is proportional to the molecular dipole moment.

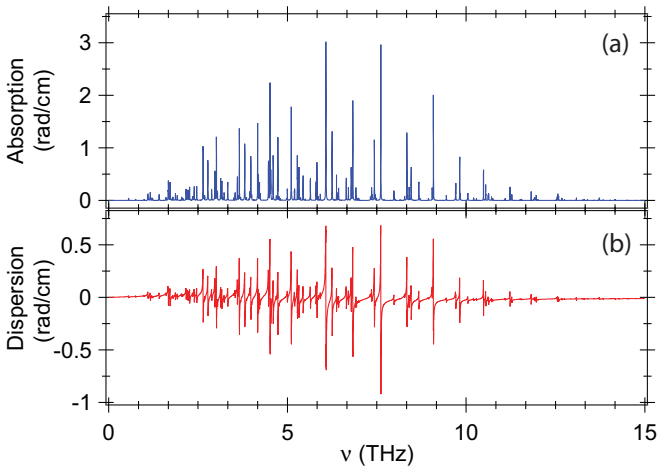

FIG. 2. Calculated absorption (a) and dispersion (b) coefficients are plotted in radians/cm as a function of the frequency. Water vapor, air pressure, and temperature are equal to 1.15×10^{-2}, 1 atm, and 296 K, respectively.

The line intensities $S_i(T)$, the transition angular frequency ω_i, and the half-widths at half maximum $\Delta\omega_i$ were retrieved from the HITRAN database [32]. Unlike the analogous calculation of Yang *et al.* [6], the use of this database [32] allows us to take into account the dependence of the linewidth on the transition being considered. The summations required to obtain the absorption and dispersion coefficients were carried out taking $J_{\mathrm{Max}} = 14$ and rotational lines within the ground (000) and first excited (010) vibrational states. This choice ensures converged results for the present investigation. Figure 2 shows the variations of the absorption and dispersion coefficients as a function of the frequency. The simulation is performed for the experimental conditions under which the FID signals were recorded, a temperature of 296 K, an air pressure of 1 atm, and a partial water pressure of 1.15×10^{-2} atm. It can be seen that the absorption spectrum is irregular due to the asymmetry of the water molecule. Moreover, owing to the fact that it is a very light molecule, its absorption spectrum spans a large frequency range of nearly 15 THz. The initial electric field at $z = 0$ was modeled using the second derivative of a Gaussian function:

$$E(0,t) = E_0(1-2at^2)\exp(-at^2), \quad (8)$$

where E_0 is the amplitude of the pulse and a is related to the pulse duration τ_{p} by $a = 6/\tau_{\mathrm{p}}^2$. The pulse duration is the time difference between the two values of t for which the electric field has its smallest (negative) values [see the inset in Fig. 3(a)]. The form taken in Eq. (8) ensures a zero time integral of the electric field. E_0 is set to 1 kV/cm (see Sec. II) and τ_{p} is fixed to the value deduced from the experimental THz pulse, i.e., 0.46 ps. The electric field $E(z,t)$ was simulated using Eq. (3). A fast Fourier transform algorithm was utilized and a time interval $[t_i,t_f]$ was chosen such that t_i is much smaller than $-\tau_{\mathrm{p}}/2$ and t_f is larger than the propagation time in the cell. Figure 3 illustrates the results of such a calculation and shows the electric field $E(z,t)$ for two propagation lengths ($z = 1$ and

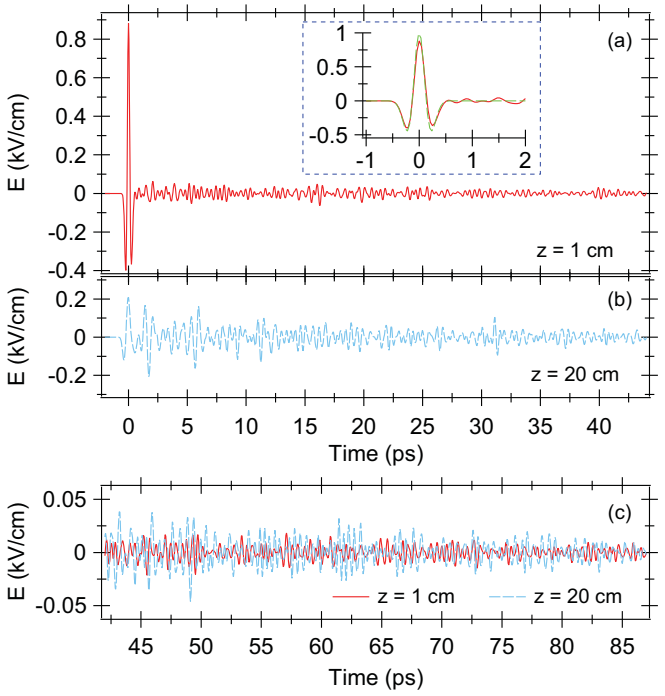

FIG. 3. Calculated variations of the electric field $E(z,t)$ for $z = 1$ cm (a, red line) and $z = 20$ cm (b, dashed blue/light-gray line). In both cases, the field is plotted as a function of the time $(t - z/c)$. A comparison with the initial THz pulse (dashed green/light gray) line around time zero is shown in the inset in panel (a). Panel (c) displays both cases at longer time. Absorption and dispersion coefficients were calculated for a temperature of 296 K, zero air pressure, and a water vapor pressure of 0.1 atm.

20 cm), a temperature of 296 K, zero air pressure, and a water vapor pressure of 0.1 atm. For $z = 1$ cm, the electric field is barely altered [Fig. 3(a)] and its shape is the one expected from Eq. (8), except for the small FID signal following the initial impulse; for $z = 20$ cm, the magnitude of the electric field is greatly reduced and its shape is altered due to the field being reradiated by the molecules [Fig. 3(b)]. The irregular nature of the absorption spectrum of the water molecule leads to a time variation much more complicated than in the case of a linear molecule [29] or a symmetric top molecule [30].

IV. RESULTS

We first analyze data recorded with the EOS detection. Figure 4 shows an experimental signal from atmospheric air with 50% humidity and a propagation length of about 39 cm, i.e., the distance from the plasma where the THz pulses are created to the ZnTe crystal where they are detected. Using the results of Sec. III, the electric field was calculated at $z = 39$ cm for a partial water pressure of 1.15×10^{-2} atm, corresponding to the above humidity, an air pressure of 1 atm, and a temperature of 296 K. A theoretical signal was calculated using Eq. (3), and taking into account two replicas of the signal due to reflections inside the ZnTe crystal (Pérot-Fabry effect). These replicas are delayed by 3.83 and 7.66 ps, respectively. The delays have been experimentally determined and agree well with the values calculated from the thickness (200 μm) and refractive index of the crystal. The results of Fig. 4 show that both phase and amplitude of the experimental signal oscillations are well reproduced by the theory.

Another recording with a longer propagation length of 302 cm in air is displayed in Fig. 5. The shape of the experimental data is also well described by calculations similar to those carried out for Fig. 4. It should be pointed out that the initial THz pulse is strongly attenuated because of a larger absorption. The agreement between observed and calculated data for this long propagation path is very similar to that observed in Ref. [6] for a transmission through 6.18 m of atmosphere and using a different database for the molecular parameters (JPL database [33]).

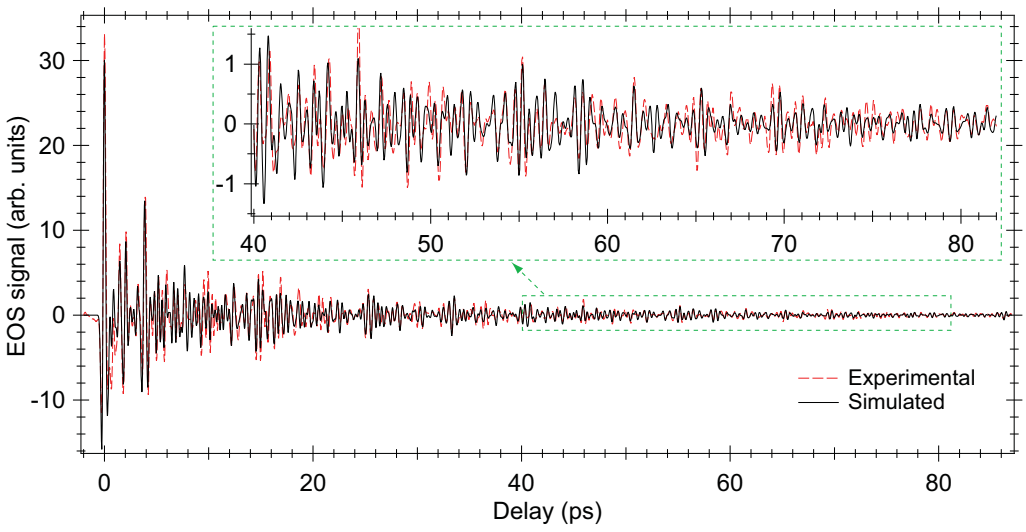

FIG. 4. Experimental (dashed red) and simulated (black line) electro-optical sampling signals S_{EOS} in air as a function of the delay between probe and THz pulses. The optical pathway is 39 cm long. Two replicas are taken into account in the simulation (see text). The simulated signal is rescaled to fit the experimental data and the delay time scale is shifted to set the origin of the time delay. A zoom of the partial trace is shown in the inset.

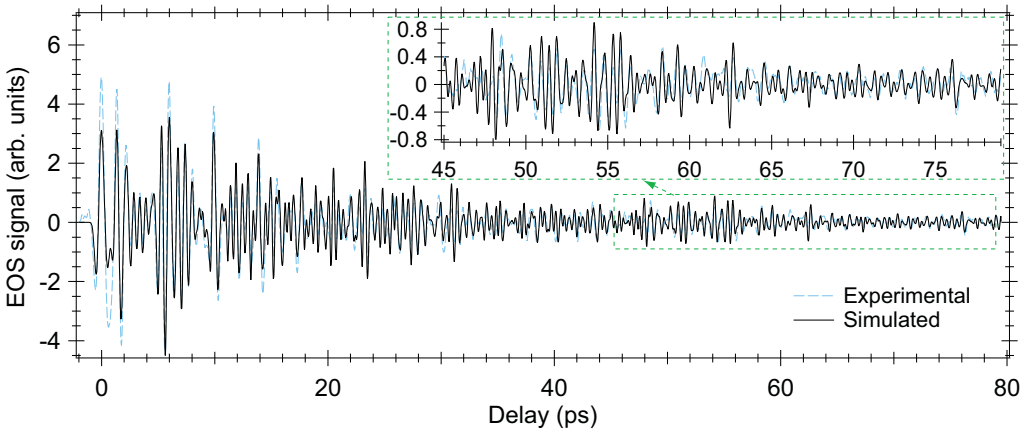

FIG. 5. Experimental (dashed blue/light gray) and simulated (black) electro-optical sampling signals S_{EOS} in air as a function of the delay between probe and THz pulses. The optical pathway is 302 cm long.

We then present measurements performed with the TFISH technique. As discussed in Sec. II, a local oscillator provided by the contribution of free electrons to the second-harmonic generation is added to the TFISH electric field. The relative magnitudes of the two contributions are adjusted by changing the probe intensity so as to obtain a good signal-to-noise ratio. Figure 6 shows a typical result for a propagation length of 39 cm. The simulated signal is fitted to the experimental data using an appropriate value for E_{LO} in Eq. (2) and a scaling factor. It should be stressed that in the case of TFISH detection, no replicas are produced, in contrast with the EOS detection. A good agreement between experimental and simulated signals is also obtained in this case. The lower signal-to-noise ratio of the TFISH experiment, in comparison with EOS detection, limits the delay range to about 30 ps. The residual discrepancy between experimental data and simulations could originate from distortion of the wave front of the THz radiation after its propagation. Indeed, at the focusing point where the THz field is measured, this wave-front distortion could lead to modification of the measured temporal shape, which does not consequently reflect accurately the actual THz field. One way to overcome this problem is generally to tightly focus, as in our case, the probe beam in order to probe only the central part of the THz beam profile. Therefore, we think that this problem should be of minimal significance in our case.

V. CONCLUSION

The FID signal of water is investigated using air at room pressure and temperature. The signal is recorded for several propagation lengths using two detection techniques presented in Sec. II. Comparison with theoretical signals is carried out based on a theoretical approach introduced in Sec. III, allowing us to account for the propagation of the electric field. The initial field is a single-cycle pulse modeled as the second derivative of a Gaussian function. Due to the complicated nature of the absorption spectrum of water, the initial pulse is modified in a complicated manner as it propagates through air. The simulations carried out for propagation lengths of 39 and 302 cm reveal that for the shorter lengths (Fig. 4) the electric field still displays a strong maximum, while for the longer length (Fig. 5) the electric field is heavily distorted. In both cases, the comparisons carried out in Sec. IV with the experimental signals are quite satisfactory. The main limitations of the two detection techniques are the presence of replicas and the limited spectral bandwidth available due to

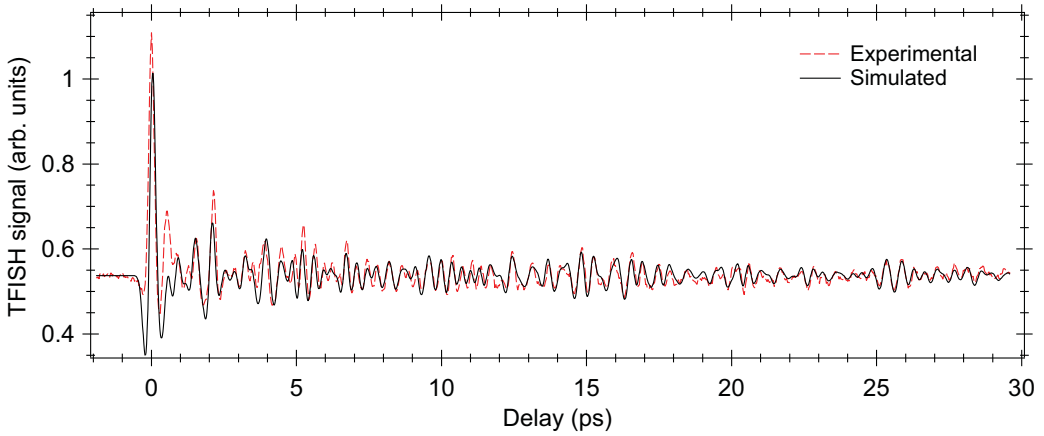

FIG. 6. Experimental (dashed red) and simulated (black) terahertz field-induced second-harmonic signals S_{TFISH} in air as a function of the delay between probe and THz pulses. The optical pathway is 39 cm long.

low-frequency phonon absorption at 1.6 and 3.7 THz [34] for EOS on the one hand, and on the other hand, the precise control of the local oscillator and the relatively low signal-to-noise ratio of TFISH compared to EOS. This work on water FID produced in atmospheric air could be extended to study the strong modulation of THz radiation at longer propagation lengths for remote sensing applications. Finally, the precise description of FID signals in molecules, in particular, in asymmetric top molecules, gives the opportunity to envision control scenarios with THz pulses. For example, the authors of Ref. [8] irradiated the OCS molecule by one single-cycle THz field followed by the FID from water. This FID provided a second THz interaction and led to strong nearly sinusoidal modulation of birefringence. These so-called commensurate two-THz revivals were produced by absorption of the 0.56-THz component of the water FID by the OCS molecule. More generally, an initial THz pulse can be shaped through propagation in a first gas cell containing a molecular sample before interacting with another molecular sample contained in a second cell. If the shaped THz pulse fits well the rotational response of the second molecule, the rotational dynamics of the latter can be controlled in the same way as described above.

ACKNOWLEDGMENTS

This work was supported by the Conseil Régional de Bourgogne (PARI program), the CNRS, the French National Research Agency (ANR) through the CoConicS program (Contract No. ANR-13-BS08-0013), and the Labex ACTION program (Contract No. ANR-11-LABX-0001-01). The authors gratefully acknowledge S. Pernot and B. Sinardet for their help in the EOS detection setup and P. Béjot for discussions.

[1] M. van Exter, C. Fattinger, and D. Grischkowsky, Opt. Lett. **14**, 1128 (1989).
[2] R. A. Cheville and D. Grischkowsky, Opt. Lett. **20**, 1646 (1995).
[3] X. Xin, H. Altan, A. Saint, D. Matten, and R. R. Alfano, J. Appl. Phys. **100**, 094905 (2006).
[4] Y. Yang, A. Shutler, and D. Grischkowsky, Opt. Express **19**, 8830 (2011).
[5] Y. Yang, M. Mandehgar, and D. Grischkowsky, Opt. Express **20**, 26208 (2012).
[6] Y. Yang, M. Mandehgar, and D. R. Grischkowsky, IEEE Trans. Terahertz Sci. Technol. **2**, 406 (2012).
[7] Y. Yang, M. Mandehgar, and D. Grischkowsky, Opt. Express **22**, 4388 (2014).
[8] S. Fleischer, R. W. Field, and K. A. Nelson, Phys. Rev. Lett. **109**, 123603 (2012).
[9] R. Damari, S. Kallush, and S. Fleischer, Phys. Rev. Lett. **117**, 103001 (2016).
[10] D. J. Cook and R. M. Hochstrasser, Opt. Lett. **25**, 1210 (2000).
[11] M. Kress, T. Löffler, S. Eden, M. Thomson, and H. G. Roskos, Opt. Lett. **29**, 1120 (2004).
[12] K. Y. Kim, J. H. Glownia, A. J. Taylor, and G. Rodriguez, Opt. Express **15**, 4577 (2007).
[13] K. Y. Kim, A. J. Taylor, J. H. Glownia, and G. Rodriguez, Nat. Photonics **2**, 605 (2008).
[14] N. V. Vvedenskii, A. I. Korytin, V. A. Kostin, A. A. Murzanev, A. A. Silaev, and A. N. Stepanov, Phys. Rev. Lett. **112**, 055004 (2014).
[15] P. Babilotte, K. Hamraoui, F. Billard, E. Hertz, B. Lavorel, O. Faucher, and D. Sugny, Phys. Rev. A **94**, 043403 (2016).
[16] C. Winnewisser, P. U. Jepsen, M. Schall, V. Schyja, and H. Helm, Appl. Phys. Lett. **70**, 3069 (1997).
[17] Y. Cai, I. Brener, J. Lopata, J. Wynn, L. Pfeiffer, J. B. Stark, Q. Wu, X. C. Zhang, and J. F. Federici, Appl. Phys. Lett. **73**, 444 (1998).
[18] G. Gallot and D. Grischkowsky, J. Opt. Soc. Am. B **16**, 1204 (1999).
[19] P. C. M. Planken, H.-K. Nienhuys, H. J. Bakker, and T. Wenckebach, J. Opt. Soc. Am. B **18**, 313 (2001).
[20] S. Fleischer, Y. Zhou, R. W. Field, and K. A. Nelson, Phys. Rev. Lett. **107**, 163603 (2011).
[21] D. Cook, J. Chen, E. Morlino, and R. Hochstrasser, Chem. Phys. Lett. **309**, 221 (1999).
[22] J. Dai, X. Xie, and X.-C. Zhang, Phys. Rev. Lett. **97**, 103903 (2006).
[23] X. Lu, N. Karpowicz, and X.-C. Zhang, J. Opt. Soc. Am. B **26**, A66 (2009).
[24] C.-Y. Li, D. V. Seletskiy, Z. Yang, and M. Sheik-Bahae, Opt. Express **23**, 11436 (2015).
[25] Y. R. Shen, Rev. Mod. Phys. **48**, 1 (1976).
[26] Y. Shen, *Principles of Nonlinear Optics* (Wiley-Interscience, New York, 1984).
[27] D. S. Bethune, Phys. Rev. A **23**, 3139 (1981).
[28] M. Beresna, P. G. Kazansky, Y. Svirko, M. Barkauskas, and R. Danielius, Appl. Phys. Lett. **95**, 121502 (2009).
[29] H. Harde and D. Grischkowsky, J. Opt. Soc. Am. B **8**, 1642 (1991).
[30] H. Harde, N. Katzenellenbogen, and D. Grischkowsky, J. Opt. Soc. Am. B **11**, 1018 (1994).
[31] P. W. Rosenkranz, J. Chem. Phys. **83**, 6139 (1985).
[32] L. S. Rothman, I. E. Gordon, Y. Babikov, A. Barbe, D. C. Benner, P. F. Bernath, M. Birk, L. Bizzocchi, V. Boudon, L. R. Brown, *et al.*, J. Quant. Spectrosc. Radiat. Transfer **130**, 4 (2013).
[33] H. Pickett, R. Poynter, E. Cohen, M. Delitsky, J. Pearson, and H. Müller, J. Quant. Spectrosc. Radiat. Transfer **60**, 883 (1998).
[34] G. Gallot, J. Zhang, R. W. McGowan, T.-I. Jeon, and D. Grischkowsky, Appl. Phys. Lett. **74**, 3450 (1999).